Using optical conductivity to detect the underlying metallic edge state in the interacting Haldane model

Can Shao [*], Hao Yuan, and Ruifeng Lu [†]

Institute of Ultrafast Optical Physics, Department of Applied Physics, Nanjing University of Science and Technology, Nanjing 210094, China

By employing the exact diagonalization method in and out of equilibrium, we investigate the half-filled spinless Haldane model on the honeycomb lattice with nearest-neighbor Coulomb repulsion. In equilibrium, the ground states with small and large interactions are in Chern insulator and charge-density-wave phase, respectively. Motivated by the recent study reporting a topologically nontrivial excited state in the strong coupling regime, we propose that such an underlying state can be detected by using optical conductivity in the open boundary condition. Specifically, we find that the dominant peak of the optical conductivity on edge is inside the bulk gap and its characteristic frequency is associated with the second excited state. Further analyses on the Drude peak indicate that the second excited state preserves a metallic edge even in the system away from the critical point. Meanwhile, it can be excited largely by not only circularly but also linearly polarized pump pulse. The latter is mostly overlooked by previous studies and implies that the polarization of the driving field is not so crucial to our system.

I. INTRODUCTION

In the past decades, the discovery of topological and Chern insulators (CIs), which fall outside the conventional Landau theory of spontaneously broken symmetry, has provided a new way for the classification of quantum phases [1–4]. There has been much effort dedicated to the relevant investigations, and topological phases of matter are now largely understood. For example, by solving single-particle Hamiltonians in non-interacting systems, topologically ordered states have been fully classified based on time-reversal, particle-hole, chiral, and crystal symmetry [5–8]. On top of that, the effects of interactions on topology also attracted much interest due to the rich and complicated physics of correlated systems [9]. Interactions themselves, on the one hand, may directly induce the so-called topological Mott insulator [10–18], especially in quadratic band crossing systems with weak interactions [19–26]. On the other hand, the interplay of topology with local orders could generate exotic states, such as the antiferromagnetic topological (or Chern) insulator [27–32]. In finite systems, the coexistence of the topological and the charge-density-wave (CDW) state is also examined even though it is strongly dependent on the lattice size and shape [33,34].

As a promising technique, nonequilibrium scenarios offer an extra dimension for the realization and modulation of exotic states. Among them, circularly polarized laser has been proposed to dynamically generate a short-lived topological state, such as light-induced anomalous Hall effect [35] and Floquet engineered topological phases in noninteracting systems [36–42]. In theory, a basic agreement is

that the topological invariant (Chern number) of the time-dependent wave function keeps unchanged under the local unitary evolution in the thermodynamic limit [43]. However, recent studies on quench and pump dynamics show that the dynamically induced Hall response may coexist with an invariant Chern number especially in interacting systems [44–47], while in equilibrium they are connecting to each other by the celebrated Thouless-Kohmoto-Nightingale-den Nijs (TKNN) formula [48].

In this paper, we study the interacting Haldane model at half filling with open boundary condition (OBC) by employing the exact diagonalization (ED) method. It is known that the interaction drives the system from CI to CDW ground state (GS) in equilibrium. Motivated by the study showing an excited state with finite Chern number in the strong coupling regime [47], we further explore the possibility to detect such an underlying state by means of optical conductivity, instead of Hall response. Through defining the spatially separated bulk and edge, we find that in the CDW regime, the dominant peak of the optical conductivity on edge locates inside the bulk gap and its frequency is consistent with the energy difference between the second excited state and GS. By careful analyses on Drude weight, we show that the second excited state still preserves a metallic edge even if the system is far from the phase transition point. After a resonant pump pulse with either linear or circular polarization applied to the CDW ground state, a large enhancement of the overlap between the time-evolving wave function and the second excited state can be observed. This feature indicates that the driving field just serves as a trigger to recover the underlying metallic edge state, while its polarization is not so crucial to our system.

The presentation is organized as follows: In Sec. II, after introducing the model Hamiltonian, a description of the numerical method we employ is presented. The results of

---
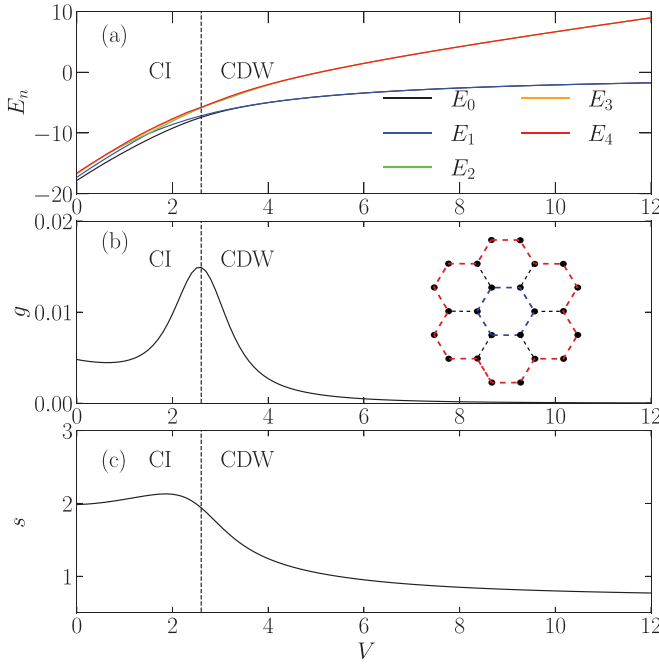[*]shaocan@njust.edu.cn
[†]rflu@njust.edu.cn

FIG. 1. Five lowest-lying energy levels (a), the ground-state fidelity metric (b), and entanglement entropy (c) vs V for the Hamiltonian (1). The inset in (b) shows the 24A cluster with open boundary condition.

optical conductivity in equilibrium and the time-dependent analyses after resonant excitation are detailed in Sec. III. Last, a conclusion is given in Sec. IV.

II. MODEL AND METHOD

The Hamiltonian we study is the half-filled spinless Haldane model with nearest-neighbor interactions:

$$\hat{H} = -t_h \sum_{\langle i,j \rangle} (\hat{c}_i^\dagger \hat{c}_j + \text{H.c.}) - t_h' \sum_{\langle\langle i,j \rangle\rangle} (e^{i\phi_{ij}} \hat{c}_i^\dagger \hat{c}_j + \text{H.c.})$$
$$+ V \sum_{\langle i,j \rangle} \hat{n}_i \hat{n}_j, \quad (1)$$

where $\hat{c}_i^\dagger$ ($\hat{c}_i$) creates (annihilates) an electron at site i and $\hat{n}_i$ is the corresponding number operator. t_h and V are the nearest-neighbor hopping constant and interaction strength, respectively. The complex next-nearest-neighbor hoppings, i.e., $t_h' e^{i\phi_{ij}}$ in anticlockwise and $t_h' e^{-i\phi_{ij}}$ in clockwise loops, induce an effective magnetic flux and break the time-reversal symmetry. The 24A cluster with OBC is adopted, as shown in the subplot of Fig. 1(b). We then define the bulk (blue dashed circle) and edge (red dashed circle) of the system, and calculate their optical conductivities. Due to the finite size of our lattice, we just treat the edge and bulk as one-dimensional periodic chains.

In equilibrium, one way to obtain the optical conductivity $\sigma(\omega)$ is from the Kubo formula [49]:

$$\sigma_{\text{reg}}(\omega) = \frac{1}{\omega L} \int_0^{+\infty} e^{i\omega t} \langle \psi_0 | [j(t), j(0)] | \psi_0 \rangle \, dt$$
$$= \frac{\pi}{L} \sum_{m \neq 0} |\langle \psi_m | j | \psi_0 \rangle|^2 \delta(\omega + E_m - E_0), \quad (2)$$

where $|\psi_0\rangle$ and $|\psi_m\rangle$ are the ground state and mth eigenstate, respectively. A spectral broadening factor $\eta = 0.1$ is introduced to the δ function. The current $j(t)$ is the Heisenberg representation of the current operator, which reads

$$j = -i t_h \sum_{i,\sigma} [c_{i,\sigma}^\dagger c_{i+1,\sigma} - \text{H.c.}]. \quad (3)$$

Here the site i is in the internal (external) circle with $L = 6$ (18) for the bulk (edge). Notice that due to $m \neq 0$, Eq. (2) only gives the regular part of the optical conductivity, i.e., $\sigma(\omega)$ with $\omega \neq 0$.

As an important quantity to characterize the metallic state, the Drude weight D is associated with the singularity of $\text{Re}\,\sigma(\omega)$ at $\omega = 0$ [50,51]:

$$\text{Re}\,\sigma(\omega) = 2\pi D \delta(\omega) + \text{Re}\,\sigma_{\text{reg}}(\omega). \quad (4)$$

Due to the inability to obtain the Drude weight from $\sigma_{\text{reg}}(\omega)$, we adopt the following method which is rigorous in the linear-response regime [52,53]:

$$\sigma(\omega) = \int_0^{t_m} \sigma(t) e^{i(\omega + i\eta)t} \, dt, \quad (5)$$

$$\sigma(t) = \frac{1}{L} \left[\langle \psi(t) | \tau | \psi(t) \rangle + \int_0^t \chi(t, t'') \, dt'' \right], \quad (6)$$

where $\tau = t_h \sum_{i,\sigma} (c_{i+1,\sigma}^\dagger c_{i,\sigma} + \text{H.c.})$ is the stress tensor operator and $\chi(t, t'') = -i\theta(t - t'') \langle \psi(0) | [j^I(t), j^I(t'')] | \psi(0) \rangle$ is the two-time susceptibility. We set $t_m = 100$ as the cutoff time in which we do the Fourier transformation. The interaction representation of the current operator $j^I(t)$ is defined as $U^\dagger(t, 0) \, j \, U(t, 0)$, with $U(t, 0)$ being the time-evolution operator. We refer to this method as nonequilibrium linear response (NLR) in the following discussions. Differences between the Kubo formula and NLR method have been detailed in Ref. [54].

Out of equilibrium, we employ the time-dependent Lanczos technique in ED [55] to evolve the many-body wave function, whose key formula is

$$|\psi(t + \delta t)\rangle = e^{-iH(t)\delta t} |\psi(t)\rangle \simeq \sum_{l=1}^M e^{-i\epsilon_l \delta t} |\phi_l\rangle \langle \phi_l | \psi(t)\rangle,$$

where ϵ_l and $|\phi_l\rangle$ are the eigenvalues and eigenvectors of the M-dimensional Krylov subspace generated in the Lanczos process, respectively. In this paper, we choose $\delta t = 0.02$ and $M = 30$ to ensure the convergence of numerical evolution. The external electric field during photoirradiation can be included into the Hamiltonian via the Peierls substitution in the hopping terms:

$$c_{i,\sigma}^\dagger c_{j,\sigma} + \text{H.c.} \rightarrow e^{i\mathbf{A}(t) \cdot (\mathbf{R}_j - \mathbf{R}_i)} c_{i,\sigma}^\dagger c_{j,\sigma} + \text{H.c.}, \quad (7)$$

where $\mathbf{A}(t) = (A_x(t), A_y(t))$ is the vector potential and

$$A_x(t) = A_{0,x} e^{-(t - t_0)^2 / 2t_d^2} \cos[\omega_0(t - t_0)],$$
$$A_y(t) = A_{0,y} e^{-(t - t_0)^2 / 2t_d^2} \sin[\omega_0(t - t_0)]. \quad (8)$$

Here the temporal envelope of $\mathbf{A}(t)$ centered at t_0 is taken to be Gaussian. The parameter t_d controls its width and ω_0 is the central frequency.

In what follows, we set parameters $t_h' = 0.2$, $\phi_{ij} = \pi/2$ and focus on zero temperature throughout the paper. Dimension of our Hilbert space is 2 704 156 for the 24-site cluster at half filling. Δt is defined to be the time difference between the pump and probe instants. In addition, we use units with $e = \hbar = 1$ and the lattice spacing $a_0 = 1$. In these units, t_h and t_h^{-1} are set to be the unit of energy and time, respectively.

III. NUMERICAL RESULTS AND DISCUSSION

We start by showing five lowest-lying energy levels as a function of V in Fig. 1(a). Instead of a level crossing separating the CI and CDW phase in the periodic boundary condition (PBC) [47], the two lowest levels merge to be nearly degenerate with V increasing in the OBC. Such a discrepancy caused by finite-size effect has been discussed in the extended Haldane-Hubbard model [34]. In addition, the energy merging between the ground state ($|\psi_0\rangle$) and first excited state ($|\psi_1\rangle$) signals the formation of the CDW phase, where $|\psi_0\rangle$ and $|\psi_1\rangle$ are the symmetric and antisymmetric solutions, respectively. That is, $|\psi_0\rangle = \frac{|1\rangle + |2\rangle}{\sqrt{2}}$ and $|\psi_1\rangle = \frac{|1\rangle - |2\rangle}{\sqrt{2}}$, where $|1\rangle$ ($|2\rangle$) represents the state with electrons only localized on sublattice A (B) in our half-filling case. It has been demonstrated that $|\psi_0\rangle$ and $|\psi_1\rangle$ are not fully degenerate in finite systems because of a spontaneous symmetry breaking [56].

The phase transition point in our model locates at $V_c = 2.6$ (dashed lines in Fig. 1), which is pinned down by the peak of fidelity metric g, see Fig. 1(b). The definition of g reads [57–59]

$$g(V) \equiv \frac{2}{N} \frac{1 - |\langle\psi_0(V)|\psi_0(V + \delta V)\rangle|}{(\delta V)^2}, \quad (9)$$

where $|\psi_0(V)\rangle$ is the ground state of $\hat{H}(V)$. The lattice size $N = 24$ and we set $\delta V = 10^{-3}$. To check if our approximation to spatially separate the bulk and edge is reasonable, we calculate the von Neumann entanglement entropy of GS between the bulk and edge subsystems $s = -\text{Tr}_B(\rho_B \ln \rho_B)$, where the reduced density matrix of bulk ρ_B is obtained by tracing the edge subsystem from the global density matrix, $\rho_B = \text{Tr}_E \rho$. Figure 1(c) shows that the entanglement entropy decreases quickly near the phase transition point with increasing V, which means the entanglement between edge and bulk is weak in the CDW phase. The reason will be discussed later.

Results of the ground-state optical conductivity obtained from the Kubo formula and NLR method are shown in Figs. 2(c)–2(f), respectively, with $V = 0$ in the left and $V = 12$ in the right panel. In equilibrium, the two methods give similar results except for the singularity at $\omega = 0$, as discussed in Sec. II. In the CI phase with $V = 0$, the dominant Drude peak (peak at $\omega = 0$) appears not only on edge but also on bulk unexpectedly, as shown in Fig. 2(e). This is because the approximation of spatially separating the bulk and edge is not suitable for the CI phase, as shown in Fig. 1(c). Meanwhile, the lattice size with negligible finite-size effect should satisfy that the bulk is bigger than the edge of the system. In spite of this, a larger Drude weight on edge can be apparently observed. Except for the Drude peak, the first peaks on the edge and bulk optical conductivity locate at the same frequency $\omega \approx 2$, which is called the optical gap in insulating phase.
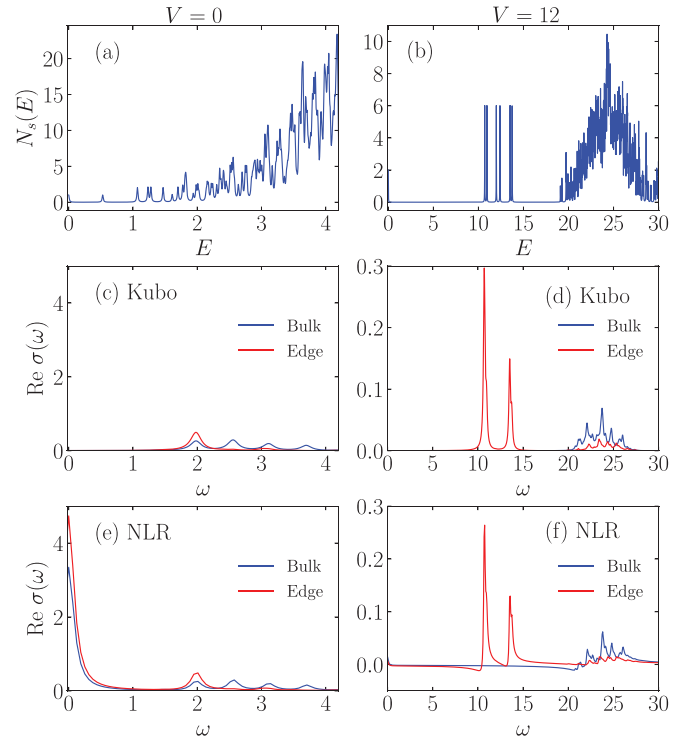

FIG. 2. Number of states $N_s(E)$ defined in Eq. (10) for $V = 0$ (a) and $V = 12$ (b). Re $\sigma(\omega)$ on the bulk (blue lines) and edge (red lines) obtained by Kubo formula (c), (d) and nonequilibrium linear response (NLR) (e), (f), with $V = 0$ in the left panel and $V = 12$ in the right panel, respectively.

While deep in the CDW phase with $V = 12$, the Drude peak is suppressed to be nearly invisible in Fig. 2(f) due to the dominating CDW order. According to our experience, it is hard to completely remove the Drude peak in a small and periodic circle even when it is in the insulating phase. What interests us is that there appear different optical gaps on bulk and edge, as shown in Figs. 2(d) and 2(f). Specifically, the dominant peaks on edge locate at $\omega \in [10, 15]$, while the major structure on bulk distributes at $\omega \in [20, 30]$, which is about twice the former. From Eq. (2), we know that peaks on the optical conductivity are associated with the excited states that can be connected to the GS by the current operator. So we calculate all the potentially relevant eigenstates with $E_n - E_0 \in [0, 30]$ and show the spectrum in Fig. 2(b). To make the spectrum more intuitive, we plot the number of states for every δE by the following formula:

$$N_s(E) = \text{Im}\left(\sum_n \frac{1}{E - (E_n - E_0) - i\delta E}\right)\delta E, \quad (10)$$

where in the sum we give a broadening factor $\delta E = 0.01$ at every discrete $E = E_n - E_0$. In short, $N_s(E)$ reflects the number of states in $[E - \delta E/2, E + \delta E/2]$.

The spectrum with $V = 12$ in Fig. 2(b) are divided into three parts:

(i) the GS and first excited state with very close energy to each other;

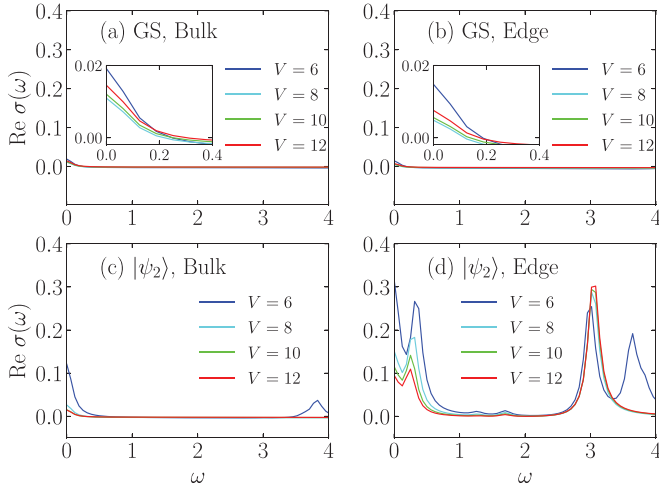(ii) 36 eigenstates from the second to 37th excited state with energy $E - E_0 \in [10, 15]$ around the value of V;

FIG. 3. Re $\sigma(\omega)$ calculated from the GS on the bulk (a) and edge (b), as well as from the second excited state on the bulk (c) and edge (d) for different V. The results are obtained by nonequilibrium linear response.
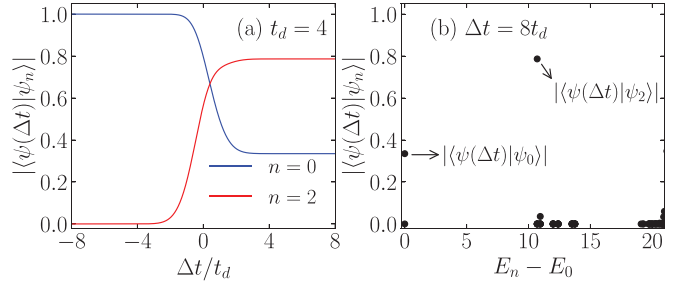

FIG. 4. (a) Time-dependent overlaps between the time-evolving wave function $|\psi(\Delta t)\rangle$ and two eigenstates $|\psi_0\rangle$ and $|\psi_2\rangle$. (b) Overlaps between $|\psi(\Delta t = 8t_d)\rangle$ and several low-energy eigenstates $|\psi_n\rangle$. The circularly polarized pump pulse with Gaussian envelope is centered at $\Delta t = 0$. Parameters: $V = 12$, $A_{0,x} = 0.1$, $A_{0,y} = 0.1$, $\omega_0 = 10.7$, and $t_d = 4.0$.

(iii) a large number of states with energy $E - E_0 \in [20, 30]$ around the value of $2V$.

It is clear that the energy scales of the last two parts are consistent with peaks on the edge and bulk optical conductivity, respectively, through comparing Figs. 2(b) and 2(d). The reason is that on honeycomb lattice with OBC, most of the sites on edge have two neighboring sites, while all sites on bulk have three neighboring sites. Roughly speaking, breaking one of the electron-hole pairs in CDW background costs V and $2V$ energies for the edge and bulk, respectively, in the strong coupling regime. This indicates that the edge will be more sensitive to external field and the CDW order inside bulk is more robust. This also leads to the rapid decreasing of entanglement entropy when the system going into the CDW phase, as shown in Fig. 1(c). Such features are absent in the CI phase because of the weak interactions, see Figs. 2(a) and 2(c). So we speculate that the second excited state $|\psi_2\rangle$, with energy $E_2 - E_0$ corresponding to the dominant peak of the edge optical conductivity, possesses a metallic edge even deep into the CDW phase. To test our idea, we analyze the conductivities of GS and $|\psi_2\rangle$.

It is worthwhile to recall that the study in PBC of this model shows that the second excited state can be smoothly connected to the original CI ground state after a level crossing and its Chern number remains $C = 1$ when $V_c < V < 4$ in the CDW regime, see Ref. [47]. However, results of the Chern number with $V > 4$ becomes invalid because of the limitation of their method. It requires that the manifold of eigenenergies of $|\psi_2\rangle$ in the torus of $E_2(\phi_x, \phi_y)$ is always gapped, where ϕ_x and ϕ_y represent the twisted phases in two directions. Instead, here we propose that a metallic edge state can be detected by analyzing the Drude weight, i.e., the optical conductivity in the low frequency. Figure 3 shows the low-frequency optical conductivity calculated from the GS on the bulk (a) and edge (b), as well as from the second excited state on the bulk (c) and edge (d), for different V in the CDW regime. Results of the GS in Figs. 3(a) and 3(b) tell us again that a tiny peak at $\omega = 0$

is unavoidable in the NLR method (check subplots therein), but it can serve as a benchmark to examine the second excited state. For $|\psi_2\rangle$, Drude peaks on the bulk are rapidly suppressed to the level of the CDW ground state with increasing V, while the low-frequency weight of the edge optical conductivity remains considerable. This feature indicates that even away from the phase transition point, i.e., $V_c = 2.6$, the second excited state keeps the metallic characteristics on edge. The above results in the optical conductivity can be compared with the Hall response in Ref. [47], where they found that the GS and $|\psi_2\rangle$ contribute zero and finite Hall response, respectively. Moreover, Hall conductance of $|\psi_2\rangle$ decreases with increasing of V, which is also consistent with the behavior of Drude weight shown in Fig. 3(d). Our results confirm that the optical conductivity in OBC and the Hall response in PBC have a very good correspondence.

Now we turn to seek the possibility to recover the underlying metallic edge state from a CDW insulator by simulating the ultrafast excitation process. We set $V = 12$ far away from the critical point, and apply the circularly polarized pump pule with parameters $A_{0,x} = 0.1$, $A_{0,y} = 0.1$, $\omega_0 = 10.7$, and $t_d = 4.0$. For resonance, ω_0 is consistent with the dominant peak of the edge optical conductivity. The amplitude A_0 and the temporal width t_d are chosen by careful analyses to better excite the second excited state. Figure 4(a) shows the time-dependent overlaps $|\langle\psi(\Delta t)|\psi_n\rangle|$, where $|\psi(\Delta t)\rangle$ is evolved from the CDW ground state under the influence of the pump centered at $\Delta t = 0$. $n = 0$ and 2 represent the GS and second excited state, respectively. We find that with the pump applied, the time-dependent wave function $|\psi(\Delta t)\rangle$ shows a decreasing overlap with the GS, while its overlap with the second excited state increases up to 0.79. After the pump, we present in Fig. 4(b) the overlaps between $|\psi(\Delta t = 8t_d)\rangle$ and several lower-energy eigenstates $|\psi_n\rangle$. It is easy to find that the second excited state is singled out by the well-tuned pump.

In experiment or noninteracting systems, the circularly polarized laser field is studied to generate topological state because it breaks the time-reversal symmetry just like the second term in Hamiltonian (1). Nevertheless, we are also interested in the linearly polarized pump pulse, which has not been studied as a way to trigger the topological state. In
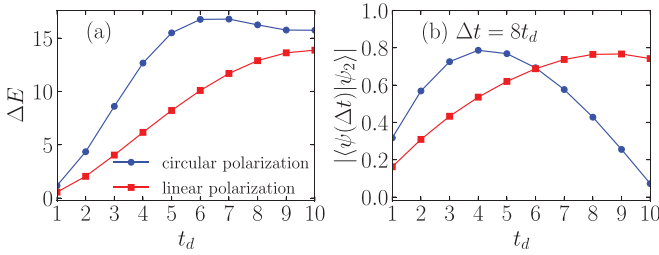
FIG. 5. (a) The injected energy ΔE (a) and overlaps between $|\psi(\Delta t = 8t_d)\rangle$ and the second excited state $|\psi_2\rangle$ (b) vs the width of pump pulse t_d. Blue and red lines represent the pump with circular and linear polarization, respectively. Parameters: $V = 12$, $A_0 = 0.1$, $\omega_0 = 10.7$.

Fig. 5(b), we plot the overlaps between $|\psi(\Delta t = 8t_d)\rangle$ and the second excited state as a function of t_d, where blue dots and red squares represent pump pulses with circular and linear polarization, respectively. We set $A_0 = 0.1$, $\omega_0 = 10.7$ and find that both kinds of pump are able to excite the second excited state to a considerable level. In addition, the circularly polarized pump requires a shorter t_d than the linearly polarized one: the optimal choice for them are $t_d = 4$ and $t_d = 8$, respectively. The reason can be attributed to the injected energy, i.e., $\Delta E = \langle\psi(\Delta t)|H(\Delta t)|\psi(\Delta t)\rangle - E_0$, where $\Delta t = 8t_d$ and E_0 is the ground-state energy. Figure 5(a) exhibits the corresponding ΔE with different t_d and implies that the optimal injected energy is $\Delta E \approx 13$. More high-energy excited states can be excited when ΔE becomes larger and thus $|\psi(\Delta t)\rangle$ lose their weight on $|\psi_2\rangle$. Our opinion is that in our system, the metallic edge state is hidden to be the second excited state due to the increase of V, and it can be triggered by both a circularly and a linearly polarized pump with appropriate injected energy.

IV. CONCLUSIONS

We investigated the half-filled spinless Haldane model with nearest-neighbor interaction V in open boundary condition. Based on the interaction strength, this model is divided into two ground-state phases, i.e., the Chern insulator and the CDW state. Deep in the CDW ground state, we observed a dominant peak on the edge optical conductivity inside the bulk gap, and its characteristic energy corresponds to the second excited state. The metallic characteristics on the edge of the second excited state is manifest based on analyses of the Drude weight. Out of equilibrium, different from previous studies using the circularly polarized laser field to break the time-reversal symmetry, the underlying metallic edge state in our system can be triggered by both circularly and linearly polarized pump pulses. Moreover, we would like to point out that the photoinduced dynamical behavior cannot be explained by the "heating effect" or thermal fluctuations, which has been detailed in Ref. [60]. That is, the resonant excitation could dynamically select the particular one of the system's excited states and lead to the generation of a nonequilibrium phase transition.

[1] T. Zhang, Y. Jiang, Z. Song, H. Huang, Y. He, Z. Fang, H. Weng, and C. Fang, Nature (London) **566**, 475 (2019).

[2] M. G. Vergniory, L. Elcoro, C. Felser, N. Regnault, B. A. Bernevig, and Z. Wang, Nature (London) **566**, 480 (2019).

[3] F. Tang, H. C. Po, A. Vishwanath, and X. Wan, Nature (London) **566**, 486 (2019).

[4] J. Kruthoff, J. de Boer, J. van Wezel, C. L. Kane, and R.-J. Slager, Phys. Rev. X **7**, 041069 (2017).

[5] A. Kitaev, AIP Conf. Proc. **1134**, 22 (2009).

[6] A. P. Schnyder, S. Ryu, A. Furusaki, and A. W. W. Ludwig, Phys. Rev. B **78**, 195125 (2008).

[7] R.-J. Slager, A. Mesaros, V. Juričić, and J. Zaanen, Nat. Phys. **9**, 98 (2013).

[8] J. C. Budich and B. Trauzettel, Phys. Status Solidi RRL **7**, 109 (2013).

[9] M. Hohenadler and F. F. Assaad, J. Phys.: Condens. Matter **25**, 143201 (2013).

[10] S. Raghu, X.-L. Qi, C. Honerkamp, and S.-C. Zhang, Phys. Rev. Lett. **100**, 156401 (2008).

[11] J. Wen, A. Rüegg, C.-C. J. Wang, and G. A. Fiete, Phys. Rev. B **82**, 075125 (2010).

[12] J. C. Budich, R. Thomale, G. Li, M. Laubach, and S.-C. Zhang, Phys. Rev. B **86**, 201407(R) (2012).

[13] A. Dauphin, M. Müller, and M. A. Martin-Delgado, Phys. Rev. A **86**, 053618 (2012).

[14] C. Weeks and M. Franz, Phys. Rev. B **81**, 085105 (2010).

[15] A. Rüegg and G. A. Fiete, Phys. Rev. B **84**, 201103(R) (2011).

[16] K.-Y. Yang, W. Zhu, D. Xiao, S. Okamoto, Z. Wang, and Y. Ran, Phys. Rev. B **84**, 201104(R) (2011).

[17] T. Yoshida, R. Peters, S. Fujimoto, and N. Kawakami, Phys. Rev. Lett. **112**, 196404 (2014).

[18] L. Wang, X. Dai, and X. C. Xie, Europhys. Lett. **98**, 57001 (2012).

[19] K. Sun, H. Yao, E. Fradkin, and S. A. Kivelson, Phys. Rev. Lett. **103**, 046811 (2009).

[20] J. M. Murray and O. Vafek, Phys. Rev. B **89**, 201110(R) (2014).

[21] J. W. F. Venderbos, M. Manzardo, D. V. Efremov, J. van den Brink, and C. Ortix, Phys. Rev. B **93**, 045428 (2016).

[22] H.-Q. Wu, Y.-Y. He, C. Fang, Z. Y. Meng, and Z.-Y. Lu, Phys. Rev. Lett. **117**, 066403 (2016).

[23] W. Zhu, S.-S. Gong, T.-S. Zeng, L. Fu, and D. N. Sheng, Phys. Rev. Lett. **117**, 096402 (2016).

[24] O. Vafek and K. Yang, Phys. Rev. B **81**, 041401(R) (2010).

[25] J. Wang, C. Ortix, J. van den Brink, and D. V. Efremov, Phys. Rev. B **96**, 201104(R) (2017).

[26] S. Uebelacker and C. Honerkamp, Phys. Rev. B **84**, 205122 (2011).

[27] R. S. K. Mong, A. M. Essin, and J. E. Moore, Phys. Rev. B **81**, 245209 (2010).

[28] C. Fang, M. J. Gilbert, and B. A. Bernevig, Phys. Rev. B **88**, 085406 (2013).

[29] T. Yoshida, R. Peters, S. Fujimoto, and N. Kawakami, Phys. Rev. B **87**, 085134 (2013).

[30] S. Miyakoshi and Y. Ohta, Phys. Rev. B **87**, 195133 (2013).

[31] T. I. Vanhala, T. Siro, L. Liang, M. Troyer, A. Harju, and P. Törmä, Phys. Rev. Lett. **116**, 225305 (2016).

[32] Y.-X. Wang and D.-X. Qi, Phys. Rev. B **99**, 075204 (2019).

[33] C. N. Varney, K. Sun, M. Rigol, and V. Galitski, Phys. Rev. B **84**, 241105(R) (2011).

[34] C. Shao, E. V. Castro, S. Hu, and R. Mondaini, Phys. Rev. B **103**, 035125 (2021).

[35] J. W. McIver, B. Schulte, F.-U. Stein, T. Matsuyama, G. Jotzu, G. Meier, and A. Cavalleri, Nat. Phys. **16**, 38 (2020).

[36] T. Oka and H. Aoki, Phys. Rev. B **79**, 081406(R) (2009).

[37] M. Bukov, L. D'Alessio, and A. Polkovnikov, Adv. Phys. **64**, 139 (2015).

[38] T. Kitagawa, T. Oka, A. Brataas, L. Fu, and E. Demler, Phys. Rev. B **84**, 235108 (2011).

[39] N. H. Lindner, G. Refael, and V. Galitski, Nat. Phys. **7**, 490 (2011).

[40] E. J. Sie, J. W. McIver, Y.-H. Lee, L. Fu, J. Kong, and N. Gedik, Nat. Mater. **14**, 290 (2015).

[41] K. Takasan, A. Daido, N. Kawakami, and Y. Yanase, Phys. Rev. B **95**, 134508 (2017).

[42] J.-i. Inoue and A. Tanaka, Phys. Rev. Lett. **105**, 017401 (2010).

[43] X. Chen, Z.-C. Gu, and X.-G. Wen, Phys. Rev. B **82**, 155138 (2010).

[44] Y. Hu, P. Zoller, and J. C. Budich, Phys. Rev. Lett. **117**, 126803 (2016).

[45] M. Schüler, J. C. Budich, and P. Werner, Phys. Rev. B **100**, 041101(R) (2019).

[46] A. Kruckenhauser and J. C. Budich, Phys. Rev. B **98**, 195124 (2018).

[47] C. Shao, P. D. Sacramento, and R. Mondaini, Phys. Rev. B **104**, 125129 (2021).

[48] D. J. Thouless, M. Kohmoto, M. P. Nightingale, and M. den Nijs, Phys. Rev. Lett. **49**, 405 (1982).

[49] R. Kubo, J. Phys. Soc. Jpn. **12**, 570 (1957).

[50] H. Castella, X. Zotos, and P. Prelovšek, Phys. Rev. Lett. **74**, 972 (1995).

[51] X. Zotos and P. Prelovšek, Phys. Rev. B **53**, 983 (1996).

[52] D. Rossini, R. Fazio, V. Giovannetti, and A. Silva, Europhys. Lett. **107**, 30002 (2014).

[53] Z. Lenarčič, D. Golež, J. Bonča, and P. Prelovšek, Phys. Rev. B **89**, 125123 (2014).

[54] C. Shao, T. Tohyama, H.-G. Luo, and H. Lu, Phys. Rev. B **93**, 195144 (2016).

[55] P. Prelovsek and J. Bonca, in *Strongly Correlated Systems-Numerical Methods*, edited by A. Avella and F. Mancini, Springer Series in Solid-State Sciences (Springer, Berlin, 2013), Vol. 176, pp. 1–30.

[56] L. Arrachea, E. R. Gagliano, and A. A. Aligia, Phys. Rev. B **55**, 1173 (1997).

[57] P. Zanardi and N. Paunković, Phys. Rev. E **74**, 031123 (2006).

[58] P. Zanardi, P. Giorda, and M. Cozzini, Phys. Rev. Lett. **99**, 100603 (2007).

[59] L. Campos Venuti and P. Zanardi, Phys. Rev. Lett. **99**, 095701 (2007).

[60] C. Shao, H. Lu, H.-G. Luo, and R. Mondaini, Phys. Rev. B **100**, 041114(R) (2019).